Journal of Geophysical Research: Earth Surface

RESEARCH ARTICLE
10.1029/2018JF004659

Morphodynamic Feedback Loops Control Stable Fringing Flats

D. C. Maan[1], B. C. van Prooijen[1], Q. Zhu[2], and Z. B. Wang[1,3]

[1]Department of Hydraulic Engineering, Delft University of Technology, Delft, The Netherlands, [2]State Key Laboratory of Estuarine and Coastal Research, East China Normal University, Shanghai, China, [3]Deltares, Delft, The Netherlands

Key Points:
- Morphodynamic feedback loops underlie the long-term dynamics and stabilization of fringing intertidal flats
- Small wind waves (5-10 cm) have a important stabilizing effect on fringing intertidal flats
- A homogeneous maximum wave-induced bed shear stress exerted by small wind waves is related with a linear cross-shore equilibrium profile

Supporting Information:
- Supporting Information S1

Correspondence to:
D. C. Maan,
d.c.maan@tudelft.nl

Citation:
Maan, D. C., van Prooijen, B. C., Zhu, Q., & Wang, Z. B. (2018). Morphodynamic feedback loops control stable fringing flats. *Journal of Geophysical Research: Earth Surface*, *123*, 2993–3012. https://doi.org/10.1029/2018JF004659

Received 1 MAR 2018
Accepted 8 OCT 2018
Accepted article online 29 OCT 2018
Published online 20 NOV 2018

Abstract We apply a 2-D horizontal process-based model (Delft3D) to study the feedback mechanisms that control the long-term evolution of a fringing intertidal flat in the Western Scheldt Estuary. The hydrodynamic model is validated using a comparison with measurements on the intertidal flat and the sediment transport module is calibrated against long-term morphology data. First, the processes that lead to net sediment exchange between channel and flat are studied. Then, long-term simulations are performed and the dependency of sediment fluxes on the tidal flat bathymetry, and the corresponding morphodynamic feedback mechanisms are explained. In the long run, relatively stable states can be approached, which are shown to be typical for wave-dominated fringing mudflats. The system behavior can be explained by the typical feedback mechanisms between the intertidal bathymetry and the hydrodynamic forces on the flat. In the subtidal domain, the impact of small (5–10 cm) wind waves increases with a rising elevation due to decreasing water depths. In the intertidal domain, the wave impact increases with increasing cross-sectional slope due to wave shoaling. These relationships result in negative (stabilizing) morphodynamic feedback loops. The tidal current velocities and tide-induced bed shear stresses, on the other hand, are largely determined by the typical horizontal geometry. A stabilizing feedback loop fails, so that there is no trend toward an equilibrium state in the absence of wind waves.

Plain Language Summary The difficulty in *managing* the long-term morphodynamics lies in the interdependencies of the underlying processes; the morphology is shaped by the hydrodynamic forces, while it influences these forces at the same time. The resulting internal feedback loops make the long-term morphodynamics difficult to model and to predict. Following a top-down approach, where we learn from the observed steady states, is a useful strategy to get toward an understanding of complex dynamical systems. This starts with realizing that an equilibrium state is not self-evident. Hence, the observation of conserved properties should naturally lead to the important question: *why are they conserved?* We apply a 2-D Delft3D model to study the feedback mechanisms that underlie the long-term evolution and stabilization of intertidal flats that fringe coastal embayments. We found that small wind waves (5–10 cm) have an important influence. Their maximum impact in shallow waters implies a strong stabilizing feedback loop in the subtidal domain, where the minimum water depth strongly increases (decreases) with a decreasing (increasing) bed level. The rest of the intertidal flat is stabilized by another feedback mechanism, induced by the process of wave shoaling and its typical dependency on the cross-sectional slope.

1. Introduction

During their flyways across the world, many migrating birds make their necessary rest stops on intertidal flats (van de Kam et al., 2010). These are gently sloped mudflats inside tidal seas or estuaries that fall dry during part of the tidal cycle, revealing a rich collection of seafood. Hence, intertidal flats are indispensable for the ecology far outside their boundaries and therefore often protected by international legislation (such as the Ramsar Convention for the protection of migratory birds and the European Natura2000 legislation).

However, loss of intertidal area, for instance, due to climate change (sea level rise) and human activities, is a common phenomenon (Airoldi & Beck, 2007; de Vet et al., 2017; Eelkema et al., 2013; Fitzgerald et al., 2008; Hoitink et al., 2017; Kirwan & Megonigal, 2013; Ma et al., 2014; Passeri et al., 2015; Sampath et al., 2011; Syvitski et al., 2005; Tambroni & Seminara, 2012). The difficulties in *managing* the long-term morphodynamics are related to the many interacting factors that play a role in the morphodynamic evolution: the (bio)morphology affects the shear stresses induced by wind waves and tidal currents, as well as the patterns of sediment transport. In turn, it is shaped by the same factors. These interactions make the morphodynamic

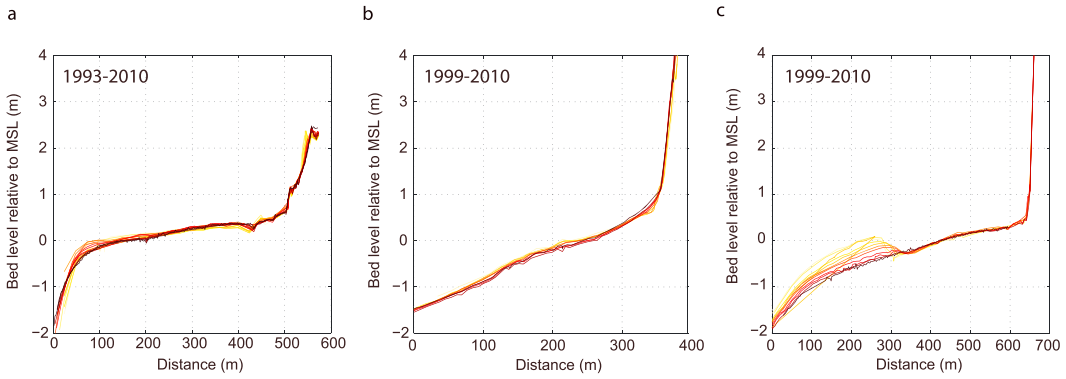

Figure 1. (a–c) Cross-shore transects of approximately stable fringing flats at respectively the locations A–C in Figure 2 (source: Rijkswaterstaat, part of the Dutch Ministry of Infrastructure and the Environment). Consecutive years are indicated from yellow to dark red over total periods of 17 (a) and 11 (b and c) years.

system behave like a *complex system* (Meadows & Wright, 2009), characterized by the occurrence of stable states (Bearman et al., 2010; Fagherazzi et al., 2006, 2007; Friedrichs, 2011; van Goor et al., 2003) and sudden transitions between these states (Wang et al., 2015).

One of the main difficulties with complex systems is that they are typically part of and built-up from other (larger and smaller scales) systems. This makes it hard to demarcate an (approximately) closed (sub)system from an overall complex system in order to split up the system into smaller and simpler parts. Hence, simplification is not always possible. Depending on the typical interactions and hierarchies inside the natural system, a system can be too big and complicated to simulate and resolve. In the field of morphodynamics, the need of high spatial and temporal resolutions in combination with large model domains and time spans easily leads to unacceptably long calculation times.

Yet to control and design the intertidal environment, and to protect it against sea level rise, we need an understanding of the system dynamics (Passeri et al., 2015; van Maanen et al., 2013). We have to discover its core and try to make a simpler, understandable, model of the real world (Zhou et al., 2017), including the dominant feedback mechanisms between the interdependent hydrodynamics, morphodynamics, and ecology.

This starts with making a careful and realistic description of the considered system and its boundaries. Boundaries need to be found that are (approximately) independent of the evolution of the modeled factors. Note that the boundary conditions do not have to represent *constant* driving factors. They can be stochastic and varying in time, as long as they behave independently from the evolution inside the model domain. In this paper, we focus on fringing intertidal flats, which are relatively easy to demarcate. These fringing intertidal areas are relatively small compared to the whole coastal or estuarine system, and even to the single adjacent channels. Due to their smaller scale, it is often possible to find model boundaries that behave (approximately) independently of the considered intertidal evolution. This gives the possibility to model these mudflats as relatively small-scale closed systems, which increases their resolvability.

Once we are able to simulate the intertidal evolution, we can look for *steady states* in the simulations. We here define the steady states as states in which certain properties of the intertidal morphology remain constant in time, controlled by negative morphodynamic feedback loops. Observations and numerical studies show that the evolution of intertidal flats often converges toward these states (Bearman et al., 2010; Fagherazzi et al., 2006, 2007; Friedrichs, 2011; Hu et al., 2015; Liu et al., 2011; Maan et al., 2015; Pritchard et al., 2002; Roberts et al., 2000). Figure 1 provides examples of approximately stable profiles for fringing intertidal flats in the Western Scheldt Estuary. Steady states can be seen as signals given by the underlying system, helpful clues to unravel its functioning. As an equilibrium state is not self-evident, the observation of conserved properties leads to the important question: *why are they conserved?* The answer to this question can reveal the whole dynamics of the system.

The kind of steady states that can be approached is characteristic for the type of intertidal system that is considered. It depends on the particular processes resulting in (net) sediment transport and the typical dependencies of these processes on the intertidal bathymetry. Earlier studies on intertidal flats that could be modeled within 0-D and 1-D frameworks indicated the dominance of feedback mechanisms between the

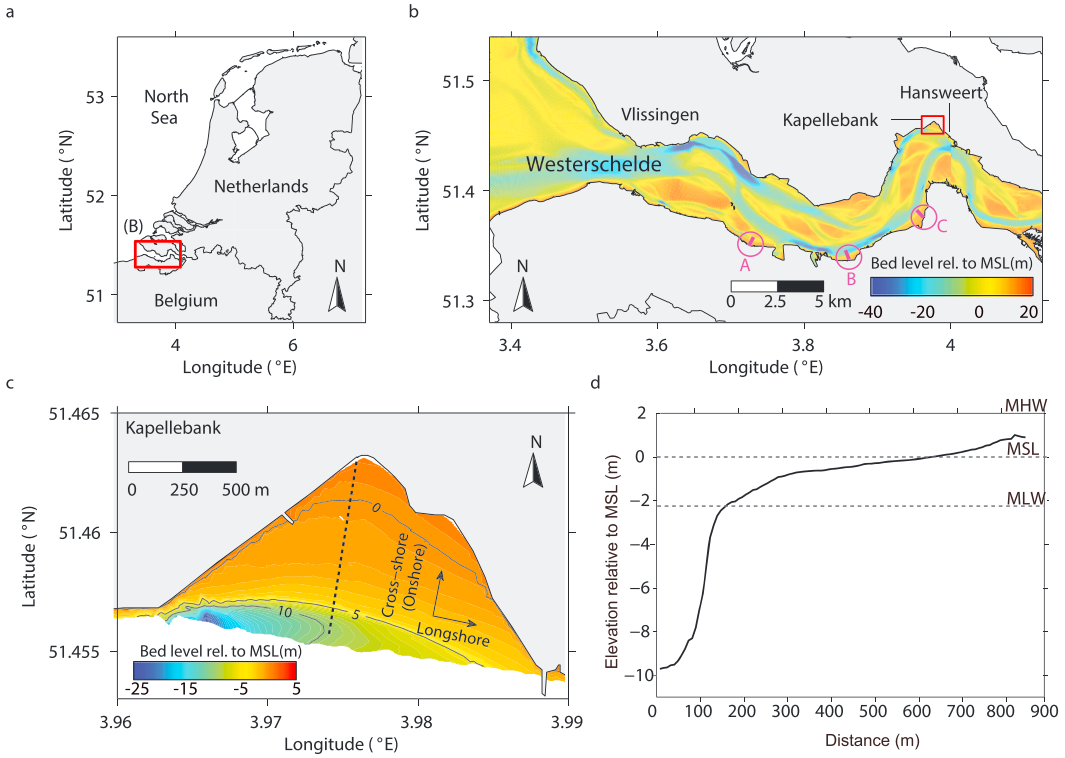

Figure 2. (a) Map of the Netherlands with the location of the Kapellebank indicated by the red square. (b) Part of the Western Scheldt Estuary with the location of the Kapellebank indicated by the red square. (c) Schematic representation of the Kapellebank. (d) A transect on the Kapellebank, indicated by the dotted line in panel c.

hydrodynamic forcing and the intertidal flat bathymetry (de Swart & Zimmerman, 2009; Fagherazzi et al., 2007; Friedrichs & Aubrey, 1996; Le Hir et al., 2000; Maan et al., 2015; Roberts et al., 2000).

Systems in which the hydrodynamic forces are controlled by locally generated wind waves, for instance, were found to converge toward horizontal platforms with a constant (equilibrium) elevation (de Swart & Zimmerman, 2009; Fagherazzi et al., 2007; Marani et al., 2007, 2010). These states are controlled by the dominance of a negative feedback loop between the bed elevation and the bed shear stress induced by locally generated wind waves (de Swart & Zimmerman, 2009; Fagherazzi et al., 2007).

Systems in which wind waves act together with cross-shore tidal currents (or in which cross-shore tidal currents act alone) were found to converge into horizontally migrating states with a conserved cross-shore profile (Maan et al., 2015; Pritchard et al., 2002; Waeles et al., 2004). These migrating states can be explained by continuous accretion on the upper intertidal flat (due to generally lower hydrodynamic energy and bed shear stresses), in combination with restoring negative feedback loops between the landward bathymetry and the cross-shore current velocities on the lower tidal flat (Maan et al., 2015).

Systems in which the hydrodynamics and sediment transport are influenced by both long-shore and cross-shore currents (i.e., those that should be described inside 2-D or 3-D frameworks) are in many ways more complicated than systems that can be resolved with a 1-D model. Inside these systems, the intertidal morphology might also have an important effect on the two-dimensional flow and advection patterns over the flat. Hence, the internal feedback mechanisms that control the long-term evolution of this kind of systems are yet to be unraveled.

In this paper, we perform a case study on the *Kapellebank*, a fringing intertidal flat at the outside of a channel bend in the Western Scheldt Estuary (The Netherlands, Figure 2). The hydrodynamic forces are induced by long- and cross-shore tidal currents and wind waves. We investigate the morphodynamic evolution of the flat with a 2-D horizontal process-based model (Delft3D). The hydrodynamic model is validated against field observations, which were carried out during a field campaign in April 2014 (see also Zhu, 2017). After the

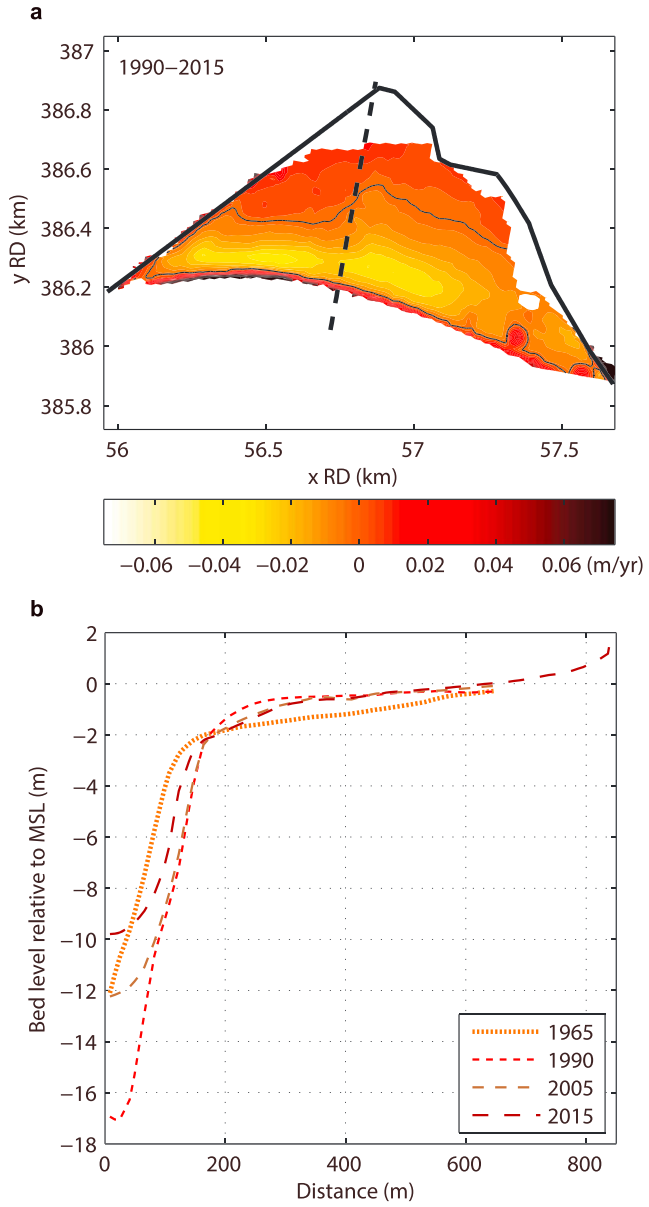

Figure 3. Observed long-term trend on the Kapellebank (based on the *Vaklodingen* data set; Wiegmann et al., 2005; see also de Vet et al., 2017). (a) Bed level differences, indicated in yearly averages (m) over the period 1990–2015. The black dashed lines indicate the position of the cross-shore transects of panel b. (b) Snapshots of the cross-shore transects in the period 1965–2015. The Kapellebank steepened over the last 25 years. In the last decade, the intertidal bathymetry is relatively stable, despite the large sedimentation rates inside the channel.

validation process, however, the boundary conditions are simplified by considering only the M2 and M4 tidal components. This is a necessary procedure for system analysis, because of the need to compare averages over closed tidal periods.

Hence, the model is applied for studying the response of an initial bathymetry to simplified boundary conditions. We are interested in how this adjustment process looks and whether or not these types of systems evolve into equilibrium states in the long run. For understanding the processes and feedback mechanisms that underlie the long-term evolution of the intertidal flat, we follow a *top-down approach*. The morphodynamic evolution is first described. Subsequently, the sedimentation rates and the hydrodynamic forces at different moments in the evolution are determined. Considering how these signals change in time and are correlated with each other reveals important information about the morphodynamic feedback mechanisms that control the evolution of the intertidal flat. Conclusions will be drawn about (1) whether steady states exist and (2) the feedback mechanisms that underlie the long-term evolution of fringing flats like the Kapellebank.

2. Study Area and Field Data

2.1. System Description: Main Actors and Driving Forces

We consider the Kapellebank, a fringing tidal flat along the north bank of the Western Scheldt Estuary in the Netherlands (Figure 2). The tidal wave is semidiurnal, with a mean tidal range of around 4 m. The flat faces a tidal channel on the south, which is delineated by a steep slope in the bathymetry (Figure 1c). Due to the close vicinity of the channel, the long-shore current dominates over the cross-shore current on the intertidal flat. However, due to the typical 2-D geometry (i.e., the location of the channel and the enclosure by the two dikes; Figure 2), the long-shore current is strongly reduced in the cross-shore direction. This is characteristic for fringing intertidal flats.

The measured cross-shore flow velocities can be compared with the analytically calculated flow velocities resulting from the filling and emptying of the intertidal volume at high tide (i.e., the tidal prism of the Kapellebank). Such a comparison reveals that only a small part (<20%) of the cross-shore currents represents the filling and emptying of the intertidal volume. Hence, this system is totally different from the ones discussed in Maan et al. (2015), Pritchard et al. (2002), and Roberts et al. (2000), where the cross-shore tidal current, caused by filling and emptying of the tidal prism of the intertidal basin, is the dominant eroding force.

The main wind direction is from the southwest, implying that the Kapellebank is often exposed to wind waves. The average wave height in the channel is about 15 cm, and the average of the highest 10% is about 30 cm. During the field campaign at the Kapellebank, wave heights were measured at the interface between the channel and the flat (Zhu, 2017). Typical values were found to be 4 cm during calm conditions and about 13 cm during strong winds (6 Bft). The sediment on the flat is cohesive, with a median grain size less than 50 μm (Guo et al., 2018; Zhu, 2017). The suspended sediment concentration in the channels of the estuary fluctuates strongly in space and time, around an average of about 40 mg/L (van der Wal et al., 2010).

2.2. Observed Trends

The channel adjacent to the Kapellebank was subject to morphological changes during the last decades; see Figure 3. Both natural processes and human interferences have influenced the channel development (Jeuken

& Wang, 2010). The change from channel erosion (1965 – 1990) to channel deposition (1990 – 2015) is to a great extent attributed to dumping activities that started around 1990 (Jeuken & Wang, 2010).

It is likely that the morphodynamic trend inside the channel influenced the morphodynamic evolution of the flat. Larger (smaller) tidal current velocities inside the channel lead to more (less) erosion at the interface between the channel and the flat. Hence, narrowing of the flat is correlated with an eroding channel and widening of the flat with an accretive channel (see Figure 3). Furthermore, variations inside the channel can affect the sediment availability: in case of an erosive channel, more sediment might be available, leading to larger accretion rates on the tidal flat. In case of an accretive channel, on the other hand, fine sediment might settle inside the channel instead (leading to smaller accretion rates on the flat). Variations in the channel might also affect the types of available sediment. Because tidal channels are generally sandier than the intertidal mudflats, an erosive channel might result in a smaller mud-sand ratio on the intertidal flat. The sediment type influences the erodability of the bed and the morphodynamic evolution of the intertidal flat (Zhu, 2017).

Despite the influence of the morphodynamically unstable adjacent channel in the past, the intertidal flat (except at its interface with the channel) is found to be rather stable over the last decade (Figure 3). Measurements on the site show that the erodibility of the bed is high (Zhu, 2017), so that the current relative stability cannot be attributed to an inactive bed. Instead, it should be explained by counteracting gross deposition and gross erosion rates.

The apparent stability of the flat suggests that the current evolution of the intertidal flat is controlled by processes that are rather independent of the morphological developments of the adjacent channel. These include the forces exerted by wind waves and sediment supply from nearby tidal flats, which is hold in suspension by tidal flow in the channel. Note that the changes inside the channel can be dominated by coarser sediment. Stable fringing intertidal flats in combination with highly dynamic (widening or narrowing) adjacent channels has also been noted by van der Wegen et al. (2017) for flats in the San Francisco Bay (see also Bearman et al., 2010).

3. The Model

3.1. Delft3D

We calculate the morphodynamic evolution of the Kapellebank with a process-based morphodynamic Delft3D model (Deltares, 2014a; Lesser et al., 2004; Roelvink, 2006), coupled to the SWAN (third generation) wave module (Booij et al., 1999; Ris et al., 1999). The flow is calculated by solving the 2-D horizontal shallow water equations (Deltares, 2014a) on a high-resolution grid with grid sizes varying from about 80 m inside the channel to less than 10 m on the Kapellebank (see Figure 4). The waves are calculated on a separate grid, with a resolution of about 10 m on the intertidal flat (Figure 4); see Deltares (2014b) for a description of the wave module.

Two-dimensional transport of suspended sediment is calculated by solving the two-dimensional advection-dispersion equation:

$$\frac{\partial ch}{\partial t} + \frac{\partial uch}{\partial x} + \frac{\partial vch}{\partial y} = \frac{\partial}{\partial x}\left(Kh\frac{\partial c}{\partial x}\right) + \frac{\partial}{\partial y}\left(Kh\frac{\partial c}{\partial y}\right) + E - D,$$

where c is the suspended sediment concentration, K is the dispersion coefficient, and E and D are the vertical erosion and deposition fluxes, respectively. These are computed by (Ariathurai, 1974; Winterwerp & Van Kesteren, 2004)

$$E = \max\left[m_e\left(\frac{\tau_b}{\tau_{cr}} - 1\right), 0\right] \quad (1)$$

and

$$D = c \cdot w_s, \quad (2)$$

where m_e is the erosion rate coefficient, τ_b the bed shear stress, τ_{cr} the critical bed shear stress for erosion, and w_s the settling velocity.

The morphodynamics of the Kapellebank are calculated for elevations above *MSL*−4 m, while the geometry and the surrounding morphology (including the bathymetry of the channel) is fixed. Because we only consider

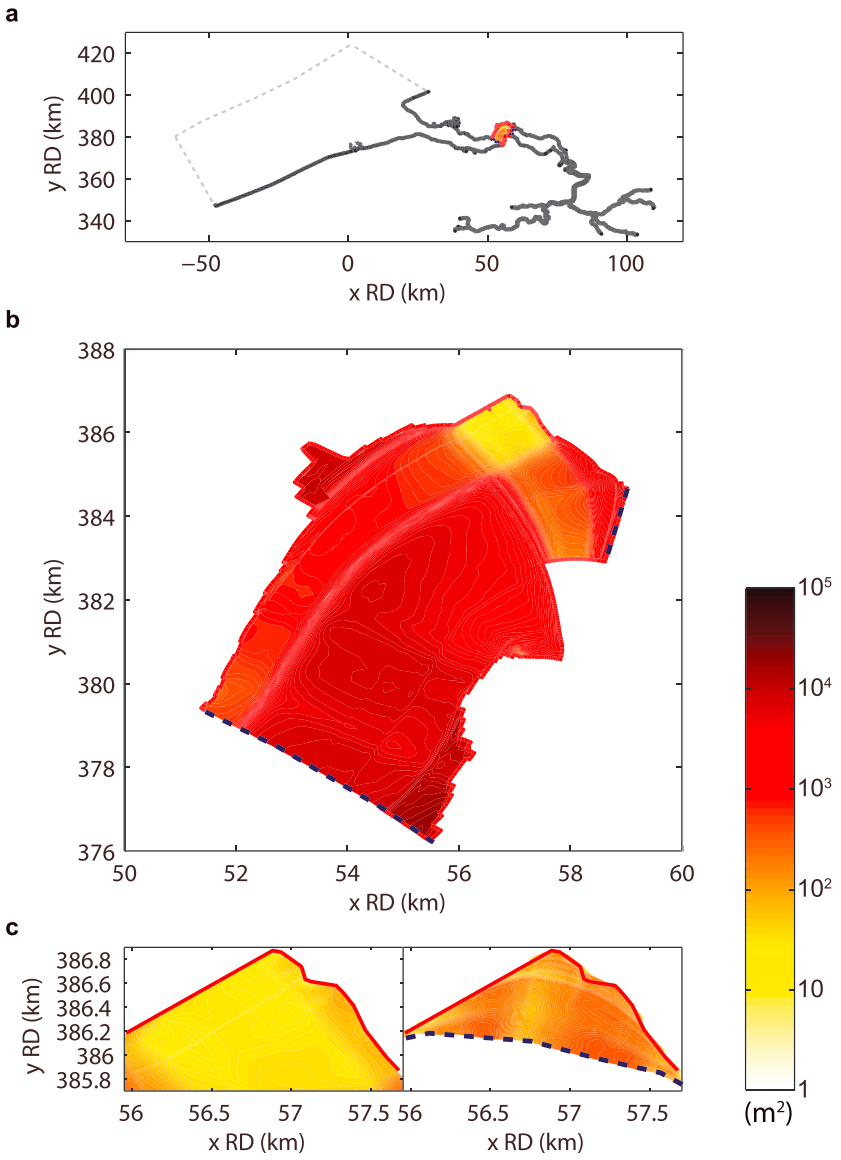

Figure 4. The closed (solid lines) and open (dotted lines) model boundaries and the grid resolution (m^2; indicated in colors) of (a) the larger-scale hydrodynamic model *Nevla* (Hartsuiker & van Banning, 2004; Maximova et al., 2009a, 2009b; Maximova, Ides, Vanlede, et al., 2009), (b) the nested flow model, and (c) a close-up view of the nested flow model (left) and the wave model (right).

changes on the flat, we use one single sediment class that represents the cohesive sediment on the flats (Zhu, 2017). The bed configuration of the Kapellebank in 2015 has been taken as initial condition. The suspended sediment concentration in the adjacent channel is controlled by applying a constant concentration at both flow model boundaries and preventing sedimentation elsewhere than on the Kapellebank.

Note that we need a high-resolution grid for calculating the complex tidal currents on the intertidal flat, which makes the calculations time-consuming. To speed up the simulation process, we apply a morphological factor (Lesser et al., 2004; Roelvink, 2006). The value of the morphological factor (Table 1) is adjusted during the simulation according to the size of the morphodynamic changes. Its effect is validated by using smaller factors at different stages of the evolution.

3.2. Boundary Conditions

The model contains two open boundaries (Figure 4). Water levels and flow velocities need to be prescribed at the southern and eastern open boundary, respectively. Naturally, the boundary conditions are assumed

Table 1
The Model Parameter Values

Parameter	Symbol	Value	Unit
Delft3D Flow			
Manning coefficient	n	0.02	$m\ s^{-\frac{1}{3}}$
Settling velocity	w_s	$0.3 \cdot 10^{-3}$	m/s
Specific density for cohesive sediment	ρ_w	2,650	kg/m^3
Dry bed density	ρ_{dry}	1,000	kg/m^3
Reference density for hindered settling	C_{ref}	1,600	kg/m^3
Horizontal eddy viscosity	ν_H	0.1	m^2/s
Horizontal eddy diffusivity	K	1	m^2/s
Critical bed shear stress for erosion	$\tau_{cr,e}$	0.35	N/m^2
Erosion coefficient	m_e	$1.7 \cdot 10^{-5}$	$kg{\cdot}m^{-2}{\cdot}s^{-1}$
Time step	Δt	3.75	s
Minimum depth for sediment calculation	h_{dry}	0.3	m
Morphological factor	M	1,000–4,000	—
Delft3D Wave			
Wave height	H	0.075–0.085	m
Wave peak period	T	2	s
Bottom roughness length scale (Madsen et al., 1988)	K_N	0.05	m

to be independent driving factors. Note that the flow through the boundaries is mainly determined by the larger-scale factors and the geometry of the estuary, so that its dependency on the bathymetry of the Kapellebank is small.

Time series of water levels and flow velocities at the southern and eastern open boundary, respectively (see Figure 4), were generated by the larger-scale model applications *Kustzuid* and *Nevla-Schelde*. These describe the hydrodynamic flow in the North Sea and through the Western Scheldt Estuary, respectively (Hartsuiker & van Banning, 2004; Maximova et al., 2009a, 2009b; Maximova, Ides, Vanlede, et al., 2009), see Eelkema et al. (2012) for a description of the Kustzuid model. These models were in turn driven by field observations. For a careful system analysis, we need to compare net sediment fluxes over closed tidal periods at different phases of the morphodynamic evolution. This procedure is much easier if we use a periodic tidal variation. Therefore, we perform a harmonic analysis on the time series and drive the model with the obtained M2 and M4 components only. The tidal amplitudes of the constituents were found the be about 1.9 m (M2) and 0.1 m (M4), with a phase difference of about 90° (small spatial variations in these values occur).

At both flow model boundaries, a constant suspended sediment concentration is imposed, which represents the background concentration. Hence, it is assumed that the fine sediment at the boundaries comes typically from the other (surrounding) tidal flats and is not significantly influenced by erosion on the Kapellebank itself. This approximation can be justified by the relative small scale of the Kapellebank, compared with the surrounding flats. Tidal variation in the sediment concentration at the boundary is not taken into account. A constant wave height, wave period (see Table 1), and wave direction (southwest) is applied at the open boundary of the wave model.

3.3. Validation and Calibration

Hydrodynamic model. The hydrodynamic model is validated against field observations. To this end, the model is forced with time series (based on field observations) of water levels and flow velocities at the southern and eastern open model boundary, respectively; see Figure 4. The model simulations are compared with field observations on the Kapellebank that were carried out by Rijkswaterstaat (part of the Dutch Ministry of Infrastructure and Environment) in May 2014. Figure 5 shows a comparison of the measured and simulated flow speeds and directions on the intertidal flat. Driven by the flow from the main channel, the flow direction is from the left flank toward the right flank during flood tide. During much of the ebb tide, the flow enters at the right flank and leaves at the left flank (see Figure 5), steered by the channel flow. In the end of the ebb

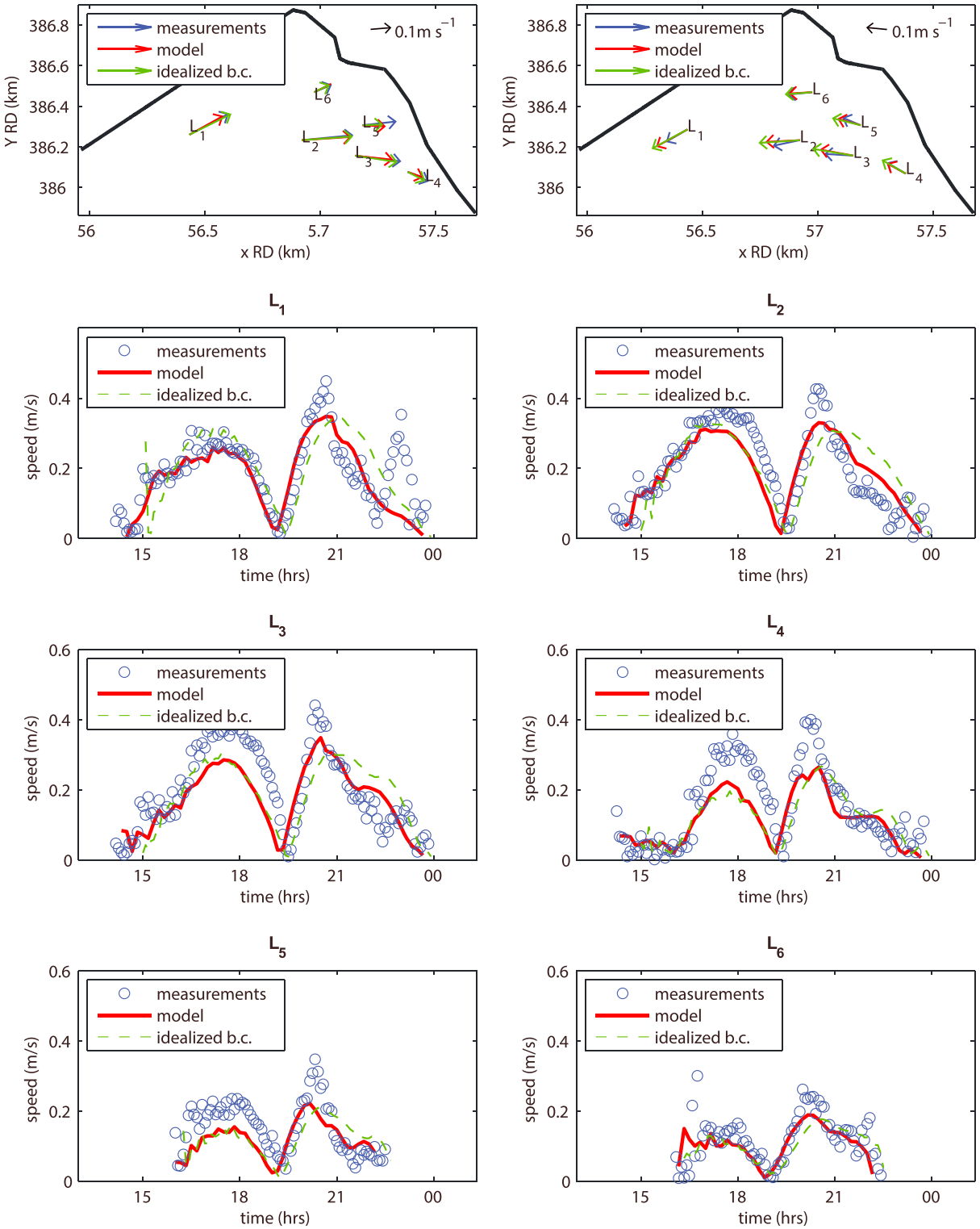

Figure 5. (top) Measured and modeled velocity vectors at the locations L1–L6 during an average tide, time-averaged over flood tide (left column) and ebb tide (right column). (bottom) Measured and modeled time series of the absolute velocity during an average tide at locations L1–L6 on the intertidal flat. The green dashed line indicates the model simulation for idealized boundary conditions, that is, including M2 and M4 tidal components only.

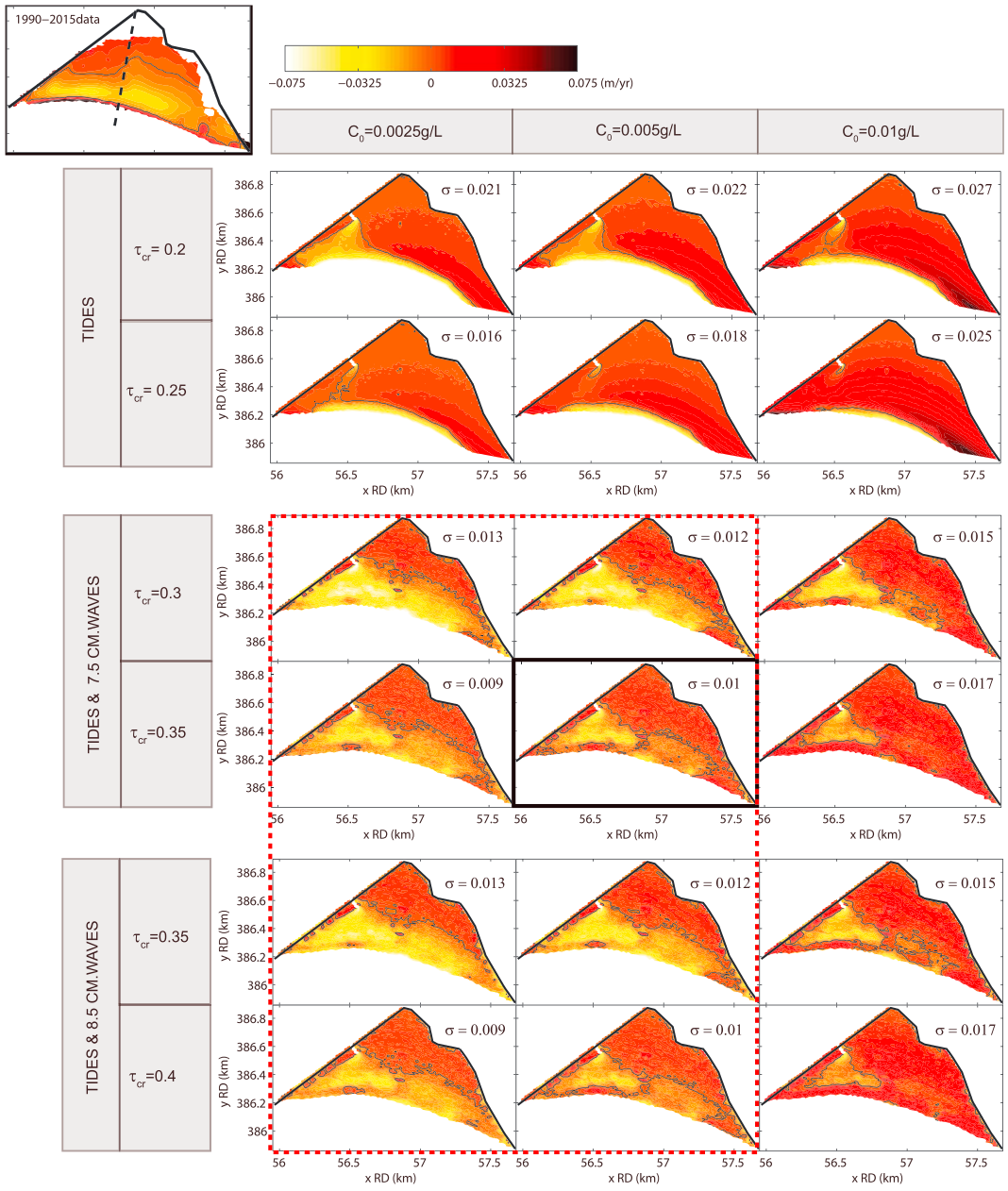

Figure 6. Modeled bed level changes over one tidal cycle (normalized to meters per year) on the present bed configuration of the Kapellebank (2015 data), for different boundary concentrations, erosion thresholds, and wave heights. The observed pattern is indicated at the top left. σ indicates the spatial average error of each simulation compared to the field data. The panels in the red dashed square are considered as *good matches*, and the parameters of the solid black surrounded panel are used for the main simulation.

tide, eddy circulations occur at the lower left flank of the flat, at the interface with the channel (see L1 in Figure 5). The ability of the model to resolve these eddies was improved by refining the grid significantly and using the Horizontal Large-Eddy Simulation subgrid module in Delft3D. For the purpose of this study, however, the faster version is applied, not including the eddy circulations. Because the eddies only occur locally, they presumably do not significantly influence the overall mudflat morphodynamics.

The capability of the model largely depends on the applied spatial resolution (Figure 4). Model parameters that influence the flow velocities over the Kapellebank are furthermore the bottom roughness (we use the setting of the Nevla model; a Manning coefficient of 0.02 m $s^{-\frac{1}{3}}$) and the horizontal eddy viscosity, which was calibrated against the field observations (determined as 0.1 m^2/s for the applied grid).

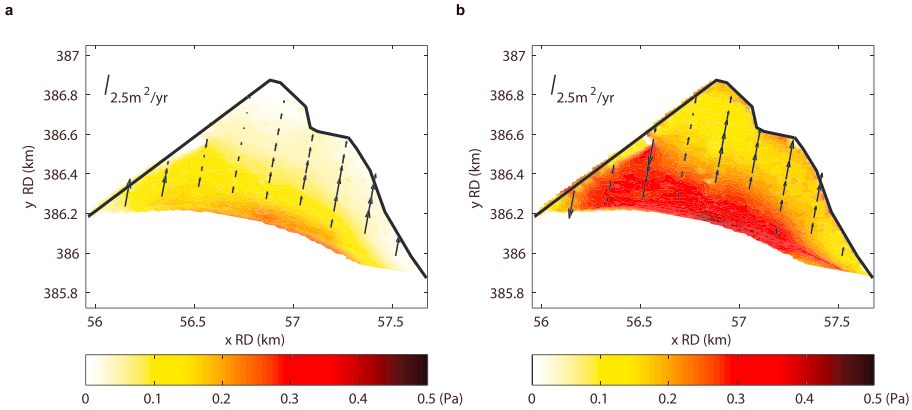

Figure 7. Maps of the tidally averaged bed shear stress (averaged over the period during which a location is flooded) and the cross-shore component of the net sediment transport per unit width (indicated by black arrows) on the current bed configuration of the Kapellebank (2015 data) in cases of (a) tidal currents only and (b) tides plus wind waves. $\tau_{cr} = 0.3$ and $C_0 = 5$ mg/L in both simulations.

Sediment transport module. Compared with the hydrodynamic module, the sediment transport module needs a more extensive calibration process. We calibrated the model against the observed long-term trend (Figure 3). To this end, simulations were performed that differ in the wave height, the wind force, the erosion threshold, the erosion coefficient, the settling velocity, and the (background) sediment concentration inside the adjacent channel. Figure 6 gives an overview of the simulated sedimentation/erosion patterns for a limited number of the applied parameter sets.

Measurement data (over the period 1990–2015) shows long-term erosion over the whole width of the lower and intermediate intertidal flat (see the top left panel of Figure 6). This pattern corresponds best with simulations that include significant wind waves, in combination with a sufficiently low boundary concentration and settling velocity (e.g., with the simulations in the red dotted box of Figure 6). The simulations without waves show too much accretion on the east side of the Kapellebank; see Figure 6. In combination with significant wind waves, the erosion threshold should be chosen sufficiently high to prevent an overestimation of the net erosion rates.

The effects of increasing the boundary concentration or the settling velocity on the sedimentation/erosion patterns were found to be rather similar to the effect of decreasing the wave height. Also, the effect of decreasing the erosion threshold was found to be comparable with the effect of increasing the wave height; see Figure 6. Hence, there exist several different parameter sets that give a fair fit with the observations.

For the main experiments, we chose the parameter values of the black surrounded panel in Figure 6. The settling velocity and wave period were taken as 0.3 mm/s and 2 s, respectively (corresponding with typical values obtained from the field measurements). To get insight into the sensitivity of the long-term morphodynamic behavior to the forcing parameters, we also performed additional long-term simulations for several different parameter sets (see sections 4.3 and 4.4). From these simulations, it followed that a careful calibration process of the parameters in Figure 6 is necessary to simulate realistic trends (see section 4.3 for a further discussion). The complete set of the model input parameters is listed in Table 1.

4. Results and Discussion

4.1. Initial Bed Shear Stress and Transport

The simulated (tidally averaged) total bed shear stress decreases toward the shore (Figure 7). Due to the presence of the channel and the orientation of the two dikes that enclose it, the long-shore current (and the tide-induced bed shear stress) is strongly reduced on the Kapellebank. The modeled wave-induced bed shear stress also shows a gradual decrease toward the shore. The shoreward decreasing bed shear stress favors net landward sediment advection (Friedrichs, 2011; Gatto et al., 2017); see Figure 7.

4.2. Feedbacks and States

Long-term morphodynamic evolution is not a simple extrapolation of the initial sedimentation patterns on a (random) initial bathymetry. Instead, the typical internal morphodynamic feedbacks can play an important

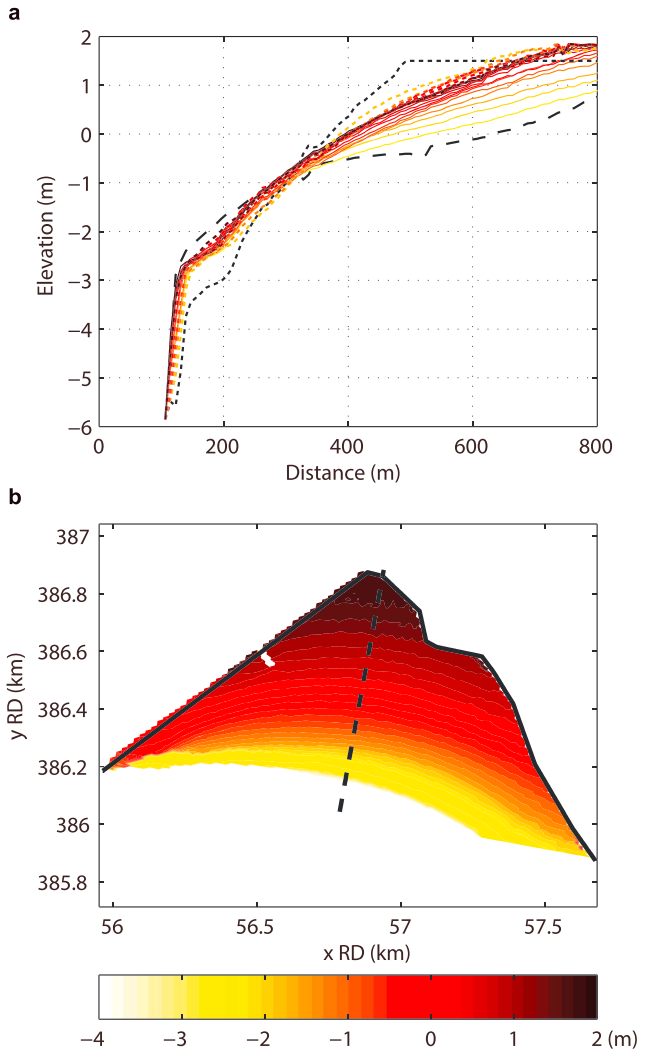

Figure 8. (a) Modeled evolution of a cross-shore transect (indicated by the dashed black line in panel b) from two different initial profiles (the dashed and dotted black lines), from yellow to dark red with time steps of 50 years and total time spans of, respectively, 600 and 350 years. The initial bathymetries are (dashed) the bed configuration from 2015 and (dotted) that mirrored around the equilibrium bathymetry. The evolutions from the dashed and dotted initial profiles are indicated by solid and dotted lines respectively. The two simulations migrate toward identical equilibrium states (indicated by the red lines). (b) Map of the equilibrium bathymetry. The applied morphological factors varied between 1,000 and 4,000; maximum values were used toward the end of the simulations.

role in the long run. Through the morphodynamic feedback loops, initial imbalances can be diminished or amplified, resulting in self-maintaining states or trends. In this section, long-term simulations are performed and studied. We try to answer the qualitative questions of (1) whether or not steady states or trends occur and, if they occur, (2) what the underlying feedback mechanisms are. The answers to these questions are often more relevant than the initial response, because they depend less on (the combination of) the initial profile and the specific model parameters and boundary conditions. They are thus less sensitive to uncertainties in these factors. In fact, the use of simplified boundary conditions is only justified when concentrating on qualitative behavior. The states or trends that we are looking for are controlled by feedback loops between the intertidal bathymetry and the hydrodynamic forces and sediment fluxes; that is, they are intrinsic properties of the system.

An equilibrium state. The long-term evolution of the Kapellebank for the calibrated parameter set is indicated in Figure 8. On the subtidal and lower intertidal flat, a balance is quickly established (within 15 years). After stabilization of the lower flat, the equilibrium state builds out landward, so that also the uppermost sections reach equilibrium eventually. The existence of an equilibrium state was further confirmed by a simulation from an alternative initial profile, which evolved into the same equilibrium state in the same chronological sequence (i.e., from the lower flat toward the shore; see Figure 8).

Now that a steady state is recognized, we can search for the underlying controlling feedback mechanisms. We first consider the correlations between changes in the bed level and changes in the bed shear stress over the morphodynamic evolution (Figure 9). On much of the intertidal flat, bed shear stresses increase (decrease) with a increasing (decreasing) bed elevation, which suggests a stabilizing feedback loop between the bed level and the local bed shear stress.

In Figure 10b it can be seen that the observed changes in the bed shear stress are mainly due to changes in the wave-induced component. Whereas the wave-induced bed shear stress on the upper flat is doubled during the morphodynamic evolution, the tide-induced bed shear stress on the equilibrium profile is almost identical to that on the initial profile (see Figure 10). This shows that the tide-induced bed shear stress is approximately independent of the intertidal bathymetry. This makes the long-shore tidal current (and its shoreward decay) an *independent driving factor*, largely determined by the typical horizontal geometry of the site. The wave-induced erosion, on the other hand, is a *state variable*, which adjusts during the bathymetric evolution.

Two wave-related processes are found to play an important stabilizing role. First, the local real-time wave-induced bed shear stress generally increases with a decreasing water depth (see Figure 11). With rising and falling tide, maximum wave-induced bed shear stresses were found close to the tidal fronts, that is, in shallow waters of less than 1 m deep (Figure 11), which corresponds with observations in the field (Zhu, 2017; see also Roberts et al., 2000). The high bed shear stresses in shallow waters effectively result in high local sediment concentration peaks that subsequently result in a dispersive sediment transport in the offshore direction. Because the tidally averaged water depth mainly decreases with an increasing bed elevation, the relationship in Figure 11 results in a negative morphodynamic feedback loop on much of the intertidal flat. This stabilizing feedback loop is particularly strong in the subtidal domain, where the minimum water depth strongly increases with an eroding bed.

Around the low water line (LWL), however, a decrease (increase) in the bed level results in a longer (shorter) period of shallow water and associated maximum bed shear stresses (because shallow water here coincides

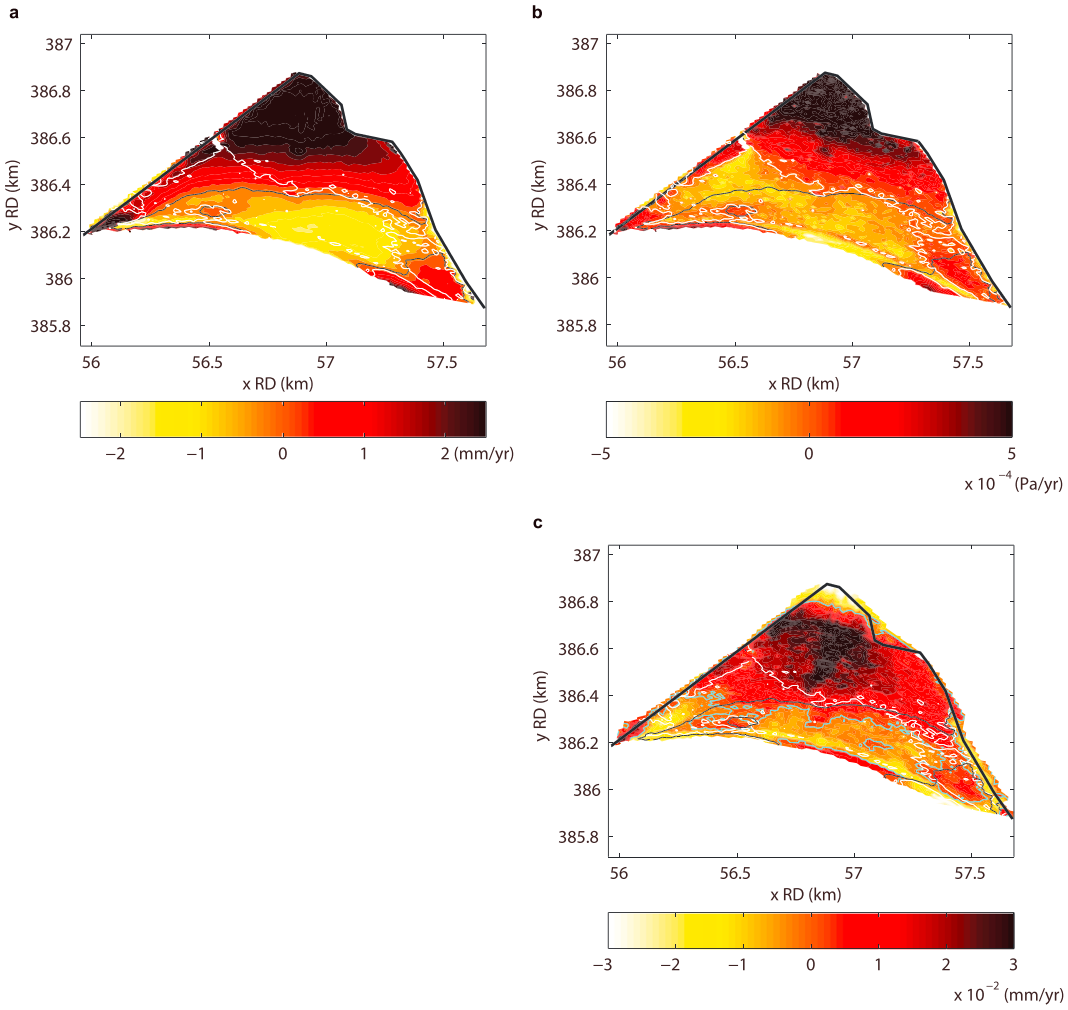

Figure 9. (a) Bed level changes over the first 300 years of the modeled evolution (accretion over time is positive), normalized to millimeters per year. (b) Corresponding changes in the tidally averaged bed shear stress (Pa/year). At most locations, the figure shows a positive correlation between the bed level and the erosion rates, which suggests a negative (stabilizing) internal feedback mechanism.(c) Corresponding changes in averaged wave height in shallow waters (less than 1 m deep), normalized to millimeters per year (with cyan zero-contour lines). (a–c) The thin black and white lines are zero-contour lines of the changes in the bed level and the erosion flux, respectively.

with slack water; see Waeles et al., 2004). Note that the bed above the LWL falls temporarily dry, whereas the bed below the LWL is wet during the whole tidal cycle. As a consequence of the longer (shorter) period of shallow water, a lowering (raising) of the bed can locally result in greater (smaller) gross erosion rates. This relationship implies a locally positive feedback loop, so that an unstable section can be expected around the LWL.

However, after the subtidal region reaches an equilibrium elevation that matches its specific supply (which is mainly determined by the sediment concentration inside the channel), another stabilizing feedback loop becomes dominant on the intertidal flat. Namely, landward of the stable section, an increase in the local bed level leads to an increase in the cross-sectional slope (in offshore direction) and thereby to an increase in the relative importance of wave shoaling versus wave dissipation (Le Hir et al., 2000). Figure 9c indicates a strong correlation between the changes in the tidally averaged erosion rates and in the wave height in shallow waters. This suggests a causal relationship; that is, the tidally averaged bed shear stress increases as a consequence of an increasing wave height in shallow waters. Hence, wave shoaling is important. Figure 12 outlines this concept.

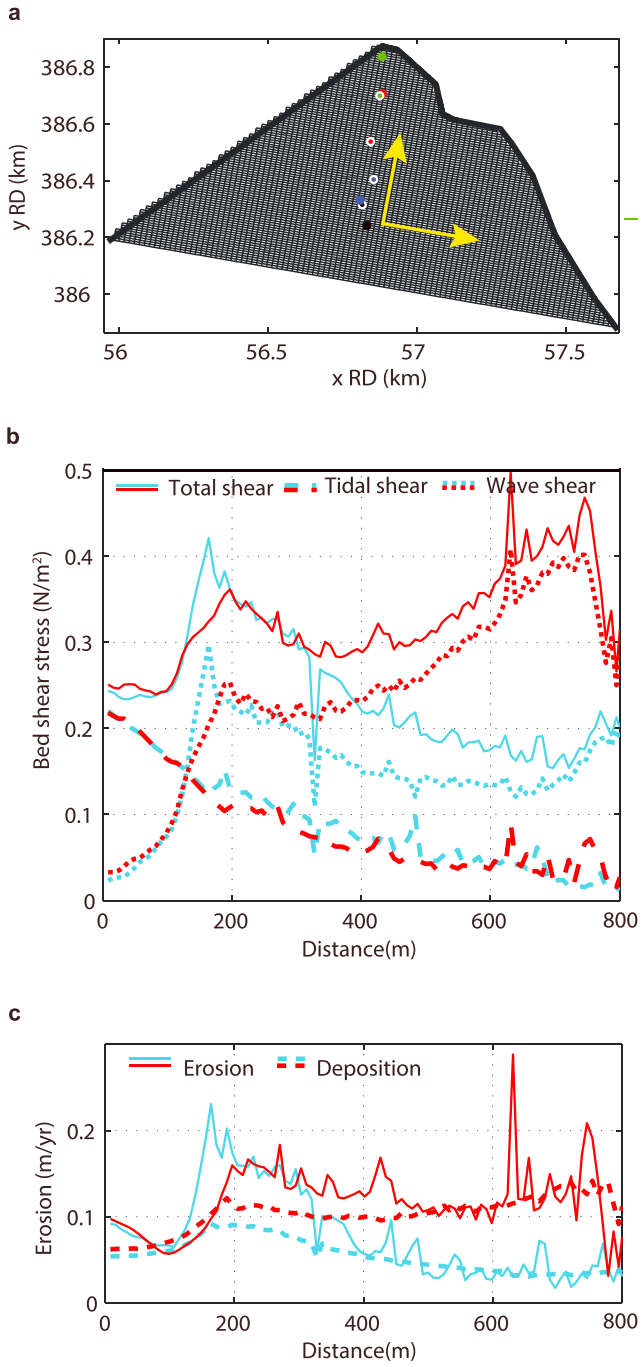

Figure 10. (a) Grid used for creation of panels b and c; the data are translated on this grid for making long-shore averages. The colored dots refer to the locations of the data in Figure 11. (b) Cross-shore variation in the bed shear stresses on the initial bathymetry (cyan) and on the equilibrium bathymetry (red), averaged over the long-shore dimension and the tidal (flooded) period. The total and tide-induced bed shear stresses are model output. The wave-induced bed shear stress is roughly estimated by the difference between these components. (c) Cross-shore variation in the gross erosion and deposition rates (m/year).

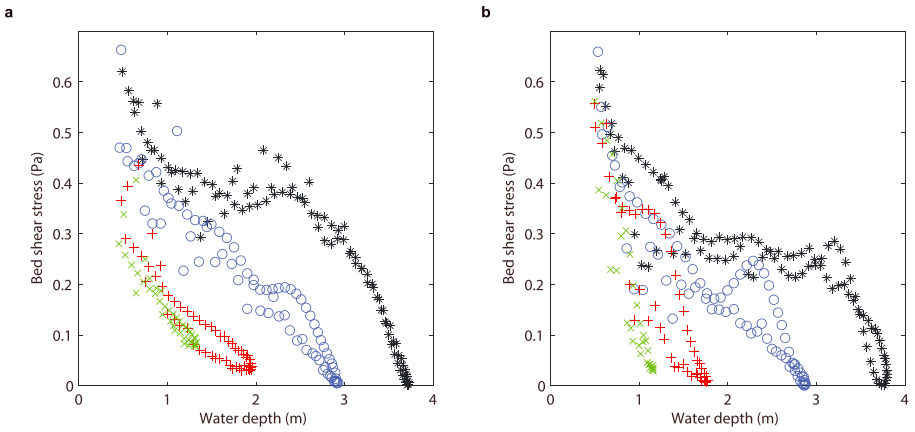

Figure 11. Modeled instantaneous total (tide-plus wave-induced) bed shear stress versus water depth during one tidal cycle at different locations, indicated with different colors and markers, on (a) the initial bathymetry and (b) the equilibrium bathymetry. The locations are indicated in Figure 10 by dots in the corresponding color. Those with white edges refer to points on the equilibrium configuration. Maximum bed shear stresses occur in shallow water. In the equilibrium state, the bed shear stresses in shallow water (less than 1m deep) are rather similar at the different locations.

The evolution toward a morphodynamic equilibrium state can now be understood as follows. The water column contains sediment that originates from a range of locations. The deposition fluxes are therefore the spatially integrated (smoothed) counterparts of the locally determined gross erosion fluxes. As a result, each location initially experiences an imbalance between the local gross erosion flux and the more global deposition flux. These imbalances naturally result in net sedimentation/erosion rates. The resulting bed level changes influence the local gross erosion fluxes, and, via the stabilizing feedback loop described in the previous paragraphs, the spatial variations in the gross erosion fluxes diminish. This process smoothens the concentration fields further, and hence, uniform conditions are approached. Uniform distributions in the tidally averaged hydrodynamic energy, erosion rates, and suspended sediment concentrations (Figure 10) minimalize the net sediment exchange by lag effects (Friedrichs, 2011; Gatto et al., 2017). Hence, despite the increase in the gross sediment fluxes on the intertidal flat, the net sediment exchange is minimalized. An equilibrium state is reached when the net horizontal sediment transport vanishes. Figure 13 shows a clear reduction in the net horizontal sediment transport. The remaining net transport in the equilibrium state (Figure 13b) balances out over multiple tidal cycles. Note that the morphodynamic feedback loops between the bathymetry and the hydrodynamic forces are subject to time lags, resulting in (small) oscillatory behavior around a steady bathymetry.

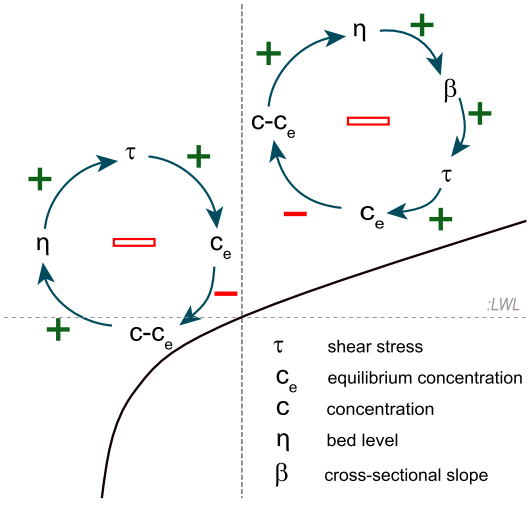

Figure 12. Feedback loops on a fringing flat. The arrows with positive and negative signs indicate positive and negative influences in between the parameters, respectively. An uneven number of negative influences within a loop results in a negative feedback loop, whereas an even number of negative influences within a loop results in a positive feedback loop. The bed levels are controlled by two balancing feedback loops, that is, if the depositon flux is initially larger than the erosion flux, that is, $c - c_e > 0$, net sedimentation occurs and the bed level rises, increasing the wave impact and the bed shear stresses, which diminishes the initial imbalance. On the intertidal flat the feedback loop between the local bed level and bed shear stress occurs via the (seaward) cross-sectional slope, due to wave shoaling.

Note that the description above is an approximation. Sediment exchange rates do not only depend on spatial gradients in the suspended sediment concentrations but also on their correlation with the flow velocities (see also Friedrichs, 2011). Bed erosion only influences the (im)balances at neighboring sections if the locally eroded sediment is transported before local settling. Although the erosion and concentration fields in the equilibrium state are found to be rather uniform, spatial variations might thus remain. Hence, the erosion rates around mean sea level can be somewhat smaller than the spatial average (see the red curve in Figure 10c), due to the locally more optimal correlation between the erosion peaks and the maximum flow advection velocities. Also, the tidally averaged concentrations on the intertidal flat are higher than those inside the tidal channel (see the red curve in Figure 10c), because a larger proportion of the eroded sediment settles locally again, instead of being exchanged. Irrespective of the specific concentration field that results in a vanishing net sediment trans-

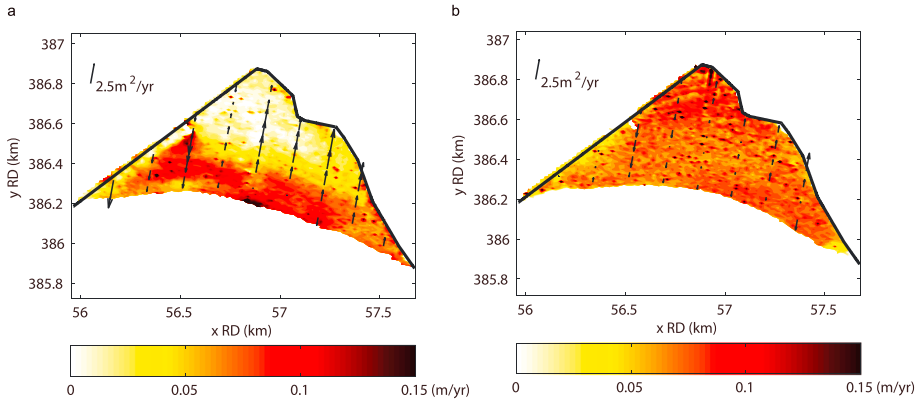

Figure 13. Maps of the tidally averaged gross erosion (translated in meters per year, indicated in colors) and the cross-shore component of the sediment transport per unit width (indicated by black arrows) on (a) the initial intertidal bathymetry and (b) the equilibrium bathymetry.

port, however, an equilibrium state can only be established via a stabilizing morphodynamic feedback loop as described above.

Due to the large exchange rate with the tidal channel via the long-shore channel flow, the *background concentration* at the lower flat is relatively independent of the upper sections, so that a balance is first established on the lower (subtidal) flat and subsequently expands landward via adjustments in the landward bathymetry (see Figure 8).

The impact of small waves. The impact of wind waves on the Kapellebank is principally different from the situation described by Friedrichs and Aubrey (1996). Friedrichs and Aubrey (1996) derived concave equilibrium profiles by assuming a homogeneous distribution of the maximum bed shear stress. Our model results confirm an (almost) uniform distribution of the maximum bed shear stress and gross erosion rates, but the profiles that we obtain are not concave. This is despite the strong dominance of the wind waves on the upper shore. The difference in the obtained equilibrium profiles can be explained by the different moment of maximum wave impact during the tidal cycle.

Friedrichs and Aubrey (1996) assumed maximum wave-induced forces during high water, when the fetch length is largest and the incoming wind waves are highest. This is probably a good assumption for higher incoming wind waves (Le Hir et al., 2000). For small wind waves (5–10 cm high), however, maximum bed shear stresses are found in shallow waters, close to the tidal fronts (Zhu, 2017; see also Roberts et al., 2000). In case of small wind waves, water depths during high tide are generally too large for optimal wave impact. The results of Le Hir et al. (2000) indicate that the section on an intertidal flat that experiences highest bed shear stresses a little after covering or before uncovering (instead of during high tide) increases with a decreasing wave height.

Hence, for small wind waves, at each moment in the tidal cycle, another location (always close to the tidal front) experiences maximum bed shear stress. The value of the maximum bed shear stress depends on the seaward bed slope via shoaling and dissipation processes. The assumption of a homogeneous distribution of the maximum bed shear stress (associated with an equilibrium state ; Friedrichs & Aubrey, 1996; see also Figure 11) therefore leads to a homogeneous slope and hence to a linear cross-sectional profile. A linear profile can thus be expected close to the shore, where the tidal currents are negligible. Its slope will depend on parameters as the sediment supply, the incoming wave height and the wave friction factor.

Note that the cross-shore transect of the modeled equilibrium state in this study (Figure 8), as well as the observed equilibrium profiles of other fringing flats in the Western Scheldt Estuary (Figure 1), is rather linear close to the shore, that is, where long-shore currents fall to 0 due to the embanked geometry. A linear equilibrium profile was also obtained by van der Wegen et al. (2017), who modeled the morphodynamic evolution of

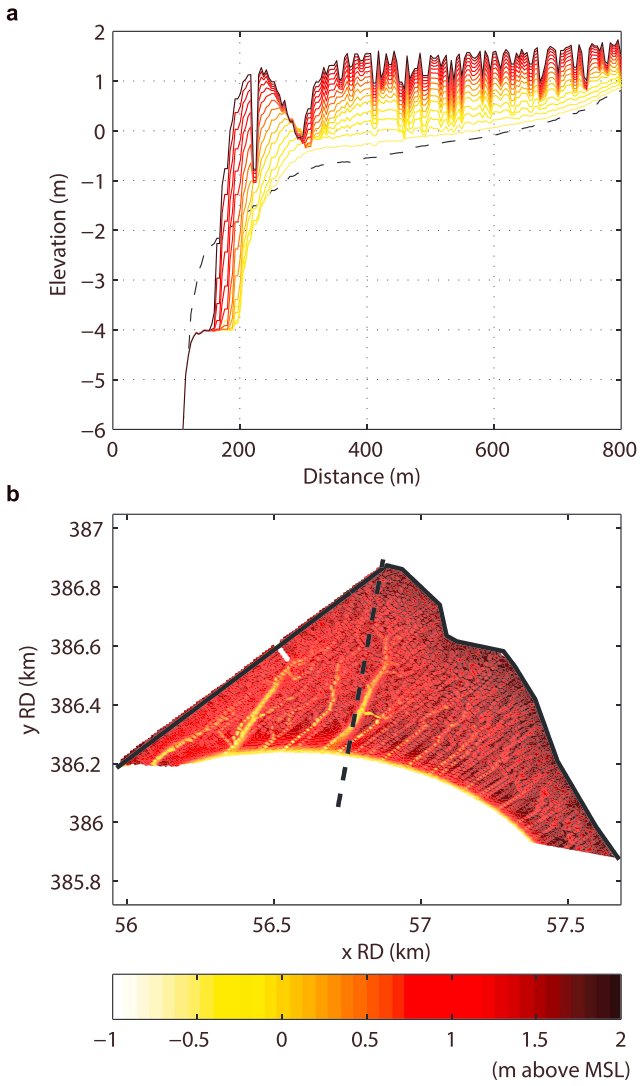

Figure 14. (a) The modeled evolution of the indicated transect in panel b, without wind waves (τ_{cr}=0.2 & C_0 = 5 mg/L). The cross-section of the initial bathymetry (2015 data) is indicated by the dashed black line and the evolution occurs from yellow toward dark red, with time intervals of 25 years and a total time span of 375 years. (b) Map of the bathymetry after 375 years of morphodynamic evolution. A morphological factor of 1,000 is applied.

a fringing flat in the San Francisco Bay with a 1-D cross-shore model including similar small wind waves (and neglecting the long-shore tidal currents).

4.3. Alternative Parameter Sets

Besides the simulation for the calibrated settings, we also considered long-term simulations for a few alternative parameter sets. From these simulations we found that the presence of wind waves does not necessarily result in an equilibrium state. In cases of a highly abundant sediment supply or a large erosion threshold, states of continuous accretion occur. In cases of low sediment availability or high wind waves, on the other hand, states of continuous erosion occur. In these cases, the feedback mechanisms are in favor of an equilibrium state, but the erosion rates on the tidal flat are never strong enough (or remain too strong) to balance out the landward sediment transport (favored by the landward decay in the tidal energy). Hence, the equilibrium state is a rather particular state and sensitive to the model parameters in Figure 6. However, equilibrium states were found for wave heights in the range 7.5–8.5 cm (with the other parameters identical to the *default* run), whereas wind waves of 9 cm resulted in an equilibrium state below the intertidal range (see see supporting information S1 for figures). Based on these results and the comparable effects of the different parameters (Figure 6), we estimate that at least the simulations within the parameter space indicated by the red dashed rectangle in Figure 6 migrate toward a stable intertidal area.

4.4. In the Absence of Wind Waves

Furthermore, we considered simulations without wind waves. In the absence of wind waves, a stationary equilibrium state is never approached (see Figure 14). The part of the intertidal flat that is initially accretive, remains accretive in the long run. The magnitudes of the net sedimentation rates on the intertidal flat decrease in the long run but are persistent. The decrease in the net sedimentation rates can be explained by a reduction in the period during which the flat is flooded, and by a decrease in the flow advection rates (which are both consequences of an increasing bed elevation). The change in advection rates affects the effectiveness of the sediment exchange between the channel and the flat (Pethick, 1981), but it cannot change the spatial concentration gradients and the direction of the net sediment transport.

For an equilibrium state (different than the total infilling or erosion of the intertidal area) to exist, a mechanism is needed by which the differences between the erosion and deposition rates, and the incoming and outgoing sediment fluxes, are diminished. A trend toward an equilibrium state would, for instance, be possible if a local increase (decrease) in the bed level would result in an increase (decrease) in the local bed shear stresses and erosion rates.

However, the spatial variation in the erosion rates is largely controlled by the horizontal two-dimensional geometry (the position of the dikes and the location of the channel), which is an independent driver. Furthermore, correlations between the bed level changes and gross erosion rates suggest a mostly positive (destabilizing) morphodynamic feedback loop between the variables (Figure 15); erosion rates on the tidal flat are decreasing with a rising bed (due to decreasing long-shore tidal flow velocities). Hence, an initial deviation from an imaginary equilibrium state would be intensified by the internal feedback loops in the system. As a consequence, a stable equilibrium state cannot exist in the absence of wind waves.

Channel formation. In the first decades, the accretion rates are maximal on the deeper parts of the intertidal area (closest to the channel), so that a flat intertidal platform is formed; see Figure 14b. This gently sloped bathymetry gives rise to the development of a structure of tidal creeks (see Figure 14a).

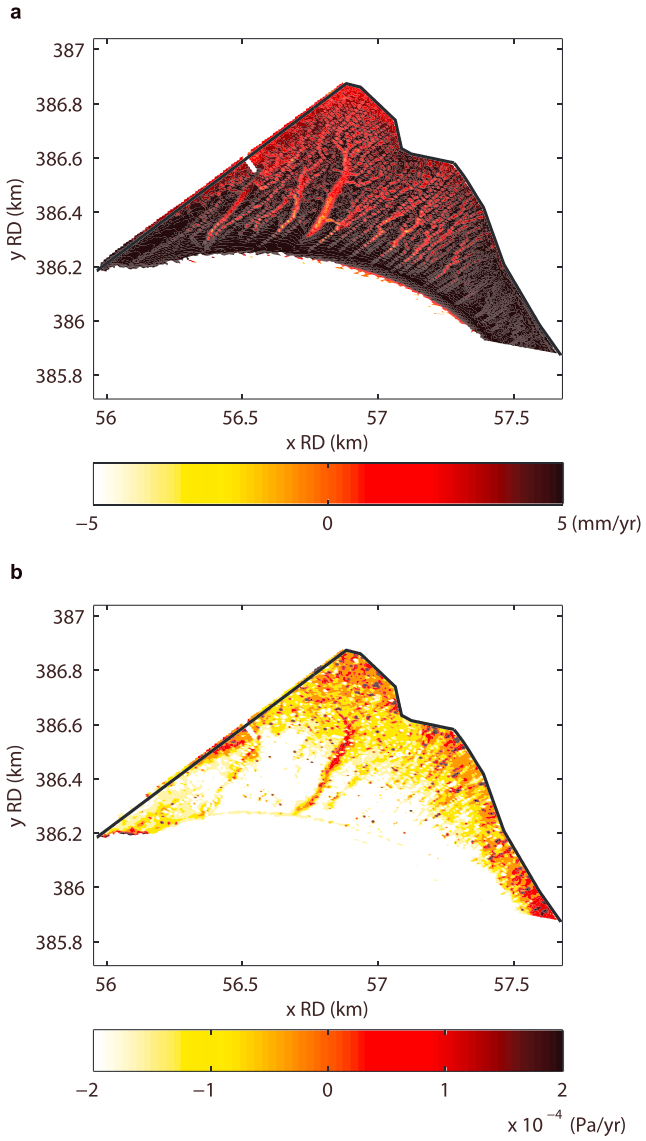

Figure 15. (a) Bed level changes (m) between 50 and 225 years of evolution (accretion over time is positive), normalized to meters per year. (b) Corresponding changes in the tidally averaged bed shear stress (Pa/year; positive values correspond with an increase in time). At most locations, the figure shows a negative correlation between the two variables, which in this case suggests a positive (destabilizing) internal feedback mechanism.

The development of the channel network is a result of a positive feedback mechanism within the intertidal system, earlier described by van Maanen et al. (2015); see Figure 15. On an uneven bed, the flow finds less resistance on the lower bed elevations where the water depth is larger. Once a weak channel structure is initiated, the flow thus concentrates through the channels, inducing relatively large flow velocities and shear stresses there, which strengthens the channel structure. At a later stage, when the structure is (locally) well-developed, a further increase of the local channel depth does not further increase the amount of water flowing through the channel. From that moment on, a further deepening of the channel leads to a decrease in the local bed shear stress (due to a larger cross-sectional area), that is, a negative feedback loop, so that the depth of the channels (relative to the surrounding flat) stabilizes (see Figure 14).

4.5. Do We Need a 2-D Model to Simulate the Equilibrium States?

Many previous studies have attempted to predict the equilibrium states of intertidal flats by 1-D cross-shore numerical and analytical models, neglecting the long-shore tidal current (Friedrichs & Aubrey, 1996; Hu et al., 2015; Maan et al., 2015; Mariotti & Fagherazzi, 2010; Pritchard et al., 2002; Roberts et al., 2000; van der Wegen et al., 2017). The results in this paper can be used to validate this approach for fringing tidal flats. The results show that the long-shore tidal current does not significantly change during the bathymetric evolution. Wave-related feedback loops, on the other hand, underlie the evolution toward an equilibrium state. This suggests that modeling of the long-shore tidal current is not strictly needed. Hence, it is expected that comparable results can be obtained by 1-D cross-shore models including wave dissipation and wave shoaling. Largest deviations can be expected on the lower flat, where long-shore tidal current velocities are largest. One-dimensional models for fringing flats can therefore be improved by including a description of the decay of the long-shore tidal current (and associated bed shear stress) in the cross-shore direction.

4.6. Battle Between Waves and Cross-Shore Tidal Currents

Opposite to the bed shear stresses induced by cross-shore tidal currents and wind waves, which co-evolve with the system as state variables, the long-shore tidal current acts (approximately) as an independent driving factor. Hence, the spatial variation in the long-shore tidal current initially determines where intertidal flats develop (i.e., at those sites where the long-shore current is relatively small/partly blocked by the typical geometry). It sets an initial energy gradient toward the shore. The energy gradient favors sediment transport (Friedrichs, 2011). In an *equilibrium state* the energy gradient induced by the long-shore tidal current is counteracted by either (1) cross-shore tidal currents or (2) wind waves. In the first case, the flat typically starts at a low elevation in the subtidal domain. The impact of wind waves is reduced by wave dissipation but can be significant in the intertidal domain. The dominance of the cross-shore tidal current in the subtidal domain, results in horizontally migrating systems (Maan et al., 2015; Mariotti & Fagherazzi, 2010; Pritchard et al., 2002).

In the second case, the mudflat starts not far below the tidal range, at the elevation where wind waves start to affect the bottom. A narrow fringing flat develops and the wave-induced feedback loops control the development toward a stationary equilibrium state. In this system, the impact of cross-shore tidal currents is negligible.

Which of these systems occur is largely determined by the combination of the available space for the flats (typically the distance between a tidal channel and a dike) and the suspended sediment concentration in the adjacent waters. These settings determine if a balance can be established in the subtidal domain by the action

of the cross-shore tidal current. Much (little) space and low (high) concentrations promote the tide (wave) controlled regime.

5. Conclusions

The bathymetry of the Kapellebank has become steeper over the last 25 years and seems rather stable during the last decade. Measurements on the site show that the erodibility of the bed is high (Zhu, 2017). Thus, the current stability cannot be attributed to an inactive bed. Instead, it should be explained by counteracting gross erosion and gross deposition rates.

Our results show that small wind waves (5–10cm) can have an important stabilizing effect on the long-term morphodynamics of the intertidal flat. For simulations without these wind waves, a stable bathymetry could not be found. The stabilizing effect of the small waves can be explained by a strong relationship between the water depth and the wave-induced bed shear stress. We found that the wave-induced bed shear stress is maximal in shallow waters (i.e., at the tidal fronts) and decreases with increasing water depth. Due to this relationship, the subtidal area stabilizes first. Subsequently, the wave-induced bed shear stress on the landward sections increases with an increasing cross-sectional slope due to wave shoaling. This implies another stabilizing morphodynamic feedback loop. By this feedback loop, the homogeneity of the gross erosion rates increases during the evolution of the flat, until the net horizontal sediment transport vanishes.

Because the tide-induced bed shear stress decreases toward the shore (which is typical for fringing flats), the equilibrium state is characterized by a shoreward increasing wave-induced bed shear stress, so as to counteract the tidal energy gradient. Closer to the shore, where the long-shore current becomes negligible, the wave-induced erosion (and maximum bed shear stress) is approximately homogeneous on the equilibrium bathymetry.

Such a homogeneous maximum wave-induced bed shear stress (exerted by small wind waves in shallow waters) is related with a linear cross-shore equilibrium profile. On a straight line, the effects of wave shoaling and wave dissipation at the tidal fronts (where the wave impact peaks) are uniform. This result differs from the concave equilibrium profiles derived analytically by Friedrichs and Aubrey (1996). Friedrichs and Aubrey (1996) assumed maximum wave-induced bed shear stresses during high water levels, representing situations with larger incoming wind waves.

Our results agree with the study by van der Wegen et al. (2017), who simulated the linear equilibrium profile of an intertidal flat in the San Francisco Bay by using a 1-D cross-shore model with similar small wind waves. Our results are also in agreement with the findings of Hunt et al. (2015) and Gatto et al. (2017). They showed on an estuarine scale that wind waves, acting on the intertidal area, are important for the establishment of an equilibrium state.

We forced our model with an average wave condition, whereas wave conditions are ever changing in reality. For stochastically varying boundary conditions, the concept of a dynamic equilibrium seems appropriate (Friedrichs, 2011; Hu et al., 2015). van der Wegen et al. (2017) noted that the ability to model a realistic evolution by average forcing only implies a system's resilience to extreme events. Our results confirm a great stability of the equilibrium configuration and provide an explanation for it. This resilience suggests that extreme events (with a sufficiently low return frequency) do not affect the long-term morphodynamics. Field observations tend to confirm the ability of the system to recover from a storm event (Zhu, 2017).

When wind waves were neglected in the simulations, a stable bathymetry was not approached. In that case, most of the flat is found to be accretive in the long run and the internal morphodynamic feedback mechanisms result in the development of tidal creeks. For the development of the tidal creeks a gentle (flat) bathymetry seems important.

Acknowledgments
We thank two anonymous reviewers, the Editors, and our colleague Stuart Pearson for their constructive comments to improve the quality of the paper. This project is supported by the Netherlands Organization for Scientific Research (NWO) via the Joint Scientific Thematic Research Programme, project 842.00.007, Fate or future of intertidal flats in estuaries and tidal lagoons. The data for producing the graphs and results are available at https://doi.org/10.4121/uuid:f7e7a85f-00ba-45c9-8b08-c2145e4e4af2.

References

Airoldi, L., & Beck, M. (2007). Loss, status and trends for coastal marine habitats of Europe. *Oceanography and Marine Biology, An Annual Review*, *45*, 345–405. https://doi.org/10.1201/9781420050943

Ariathurai, C. R (1974). A finite element model for sediment transport in estuaries (PhD thesis). Berkeley, CA: University of California.

Bearman, J. A., Friedrichs, C. T., Jaffe, B. E., & Foxgrover, A. C (2010). Spatial trends in tidal flat shape and associated environmental parameters in South San Francisco Bay. *Journal of Coastal Research*, *262*, 342–349. https://doi.org/10.2112/08-1094.1

Booij, N., Ris, R. C., & Holthuijsen, L. H (1999). A third-generation wave model for coastal regions: 1. Model description and validation. *Journal of Geophysical Research*, *104*, 7649–7666.

de Swart, H. E., & Zimmerman, J. T. F. (2009). Morphodynamics of tidal inlet systems. *Annual Review of Fluid Mechanics*, *41*(1), 203–229. https://doi.org/10.1146/annurev.fluid.010908.165159

de Vet, P. L. M., van Prooijen, B. C., & Wang, Z. B. (2017). The differences in morphological development between the intertidal flats of the Eastern and Western Scheldt. *Geomorphology*, *281*, 31–42. https://doi.org/10.1016/j.geomorph.2016.12.031

Deltares (2014a). Delft3D flow user manual. Retrieved from http://oss.deltares.nl/web/delft3d/manuals. Date accessed: 29 june 2018.

Deltares (2014b). Delft3D wave user manual. Retrieved from http://oss.deltares.nl/web/delft3d/manuals. Date accessed: 29 june 2018.

Eelkema, M., Wang, Z. B., Hibma, A., & Stive, M. J. F (2013). Morphological effects of the Eastern Scheldt storm surge barrier on the ebb-tidal delta. *Coastal Engineering Journal*, *55*(3). https://doi.org/10.1142/S0578563413500101

Eelkema, M., Wang, Z. B., & Stive, M. J. F. (2012). Impact of back-barrier dams on the development of the ebb-tidal delta of the Eastern Scheldt. *Journal of Coastal Research*, *285*, 1591–1605. https://doi.org/10.2112/JCOASTRES-D-11-00003.1

Fagherazzi, S., Carniello, L., D'Alpaos, L., & Defina, A. (2006). Critical bifurcation of shallow microtidal landforms in tidal flats and salt marshes. *Proceedings of the National Academy of Sciences of the United States of America*, *103*(22), 8337–8341. https://doi.org/10.1073/pnas.0508379103

Fagherazzi, S., Palermo, C., Rulli, M. C., Carniello, L., & Defina, A. (2007). Wind waves in shallow microtidal basins and the dynamic equilibrium of tidal flats. *Journal of Geophysical Research*, *112*, F0204. https://doi.org/10.1029/2006JF000572

Fitzgerald, D. M., Fenster, M. S., Argow, B. A., & Buynevich, I. V. (2008). Coastal impacts due to sea-level rise. *Annual Review of Earth and Planetary Sciences*, *36*(1), 601–647. https://doi.org/10.1146/annurev.earth.35.031306.140139

Friedrichs, C. T. (2011). Tidal flat morphodynamics: A synthesis. In E. Wolanski & D. McLusky (Eds.), *Treatise on estuarine and coastal science* (pp. 137–137). Waltham: Academic Press. https://doi.org/10.1016/B978-0-12-374711-2.00307-7

Friedrichs, C. T., & Aubrey, D. G. (1996). Uniform bottom shear stress and equilibrium hyposometry of intertidal flats. In C. Pattiaratchi (Ed.), *Mixing in estuaries and coastal seas, coastal and estuarine studies* (Vol. 50, pp. 405–429). Washington, DC: American Geophysical Union. https://doi.org/10.1029/CE050p0405

Gatto, V. M., van Prooijen, B. C., & Wang, Z. B (2017). Net sediment transport in tidal basins: quantifying the tidal barotropic mechanisms in a unified framework. *Ocean Dynamics*, *67*(11), 1385–1406. https://doi.org/10.1007/s10236-017-1099-3

Guo, C., Qing, H., van Prooijen, B. C., Guo, L., Manning, A. J., & Bass, S. (2018). Investigation of flocculation dynamics under changing hydrodynamic forcing on an intertidal mudflat. *Marine Geology*, *395*, 120–132. https://doi.org/10.1016/j.margeo.2017.10.001

Hartsuiker, G., & van Banning, G. K. F. M. (2004). 2Dh Nevla-Scheldemodel (SCALWEST 2000 met verbeterde Belgische roosterschematisatie): Bouw en afregeling stromingsmodel. WL Rapporten.

Hoitink, A. J. F., Wang, Z. B., Vermeulen, B., Huismans, Y., & Kästner, K. (2017). Tidal controls on river delta morphology. *Nature Geoscience*, *10*(9), 637. https://doi.org/10.1038/NGEO3000

Hu, Z., Wang, Z. B., Zitman, T. J., Stive, M. J. F., & Bouma, T. J. (2015). Predicting long-term and short-term tidal flat morphodynamics using a dynamic equilibrium theory. *Journal of Geophysical Research: Earth Surface*, *120*, 1803–1823. https://doi.org/10.1002/2015JF003486

Hunt, S., Bryan, K. R., & Mullarney, J. C. (2015). The influence of wind and waves on existence of stable intertidal morphology in meso-tidal estuaries. *Geomorphology*, *228*, 158–174. https://doi.org/10.1016/j.geomorph.2014.09.001

Jeuken, M. C. J. L., & Wang, Z. B. (2010). Impact of dredging and dumping on the stability of ebb-flood channel systems. *Coastal Engineering*, *57*(6), 553–566. https://doi.org/10.1016/j.coastaleng.2009.12.004

Kirwan, M. L., & Megonigal, J. P. (2013). Tidal wetland stability in the face of human impacts and sea-level rise. *Nature*, *504*(7478), 53–60. https://doi.org/10.1038/nature12856

Le Hir, P., Roberts, W., Cazaillet, O., Christie, M., Bassoullet, P., & Bacher, C. (2000). Characterization of intertidal flat hydrodynamics. *Continental Shelf Research*, *20*(12-13), 1433–1459. https://doi.org/10.1016/S0278-4343(00)00031-5

Lesser, G. R., Roelvink, J. A., van Kester, J. A. T. M., & Stelling, G. S (2004). Development and validation of a three-dimensional morphological model. *Coastal Engineering*, *51*(8-9), 883–915. https://doi.org/10.1016/j.coastaleng.2004.07.014

Liu, X. J., Gao, S., & Wang, Y. P. (2011). Modeling profile shape evolution for accreting tidal flats composed of mud and sand: A case study of the central Jiangsu coast, China. *Continental Shelf Research*, *31*, 1750–1760. https://doi.org/10.1016/j.csr.2011.08.002

Ma, Z., Melville, D. S., Liu, J., Chen, Y., Yang, H., Ren, W., et al. (2014). Rethinking China's new great wall. *Science*, *346*(6212), 912–914. https://doi.org/10.1126/science.1257258

Maan, D. C., van Prooijen, B. C., Wang, Z. B, & de Vriend, H. J. (2015). Do intertidal flats ever reach equilibrium? *Journal of Geophysical Research: Earth Surface*, *120*, 2406–2436. https://doi.org/10.1002/2014JF003311

Madsen, O., Poon, Y.-K., & Graber, H. (1988). Spectral wave attenuation by bottom friction: Theory. *Coastal Engineering Proceedings*, *21*, 492–504. https://icce-ojs-tamu.tdl.org/icce/index.php/icce/article/view/4241

Marani, M., D'Alpaos, A., Lanzoni, S., Carniello, L., & Rinaldo, A. (2007). Biologically-controlled multiple equilibria of tidal landforms and the fate of the Venice lagoon. *Geophysical Research Letters*, *34*, L11402. https://doi.org/10.1029/2007GL030178

Marani, M., D'Alpaos, A., Lanzoni, S., Carniello, L., & Rinaldo, A. (2010). The importance of being coupled: Stable states and catastrophic shifts in tidal biomorphodynamics. *Journal of Geophysical Research*, *115*, F04004. https://doi.org/10.1029/2009JF001600

Mariotti, G., & Fagherazzi, S (2010). A numerical model for the coupled long-term evolution of salt marshes and tidal flats. *Journal of Geophysical Research*, *115*, F01004. https://doi.org/10.1029/2009JF001326

Maximova, T., Ides, S., De Mulder, T., & Mostaert, F. (2009a). LTV O&M thema Veiligheid Deelproject 1: Verbetering hydrodynamisch NeVla model ten behoeve van scenarioanalyse. WL Rapporten, 756_05. Flanders Hydraulics Research & Deltares, Antwerp, Belgium. Retrieved from http://www.vliz.be/nl/open-marien-archief?module=ref&refid=142561&printversion=1&dropIMIStitle=1.

Maximova, T., Ides, S., De Mulder, T., & Mostaert, F. (2009b). Verbetering randvoorwaardenmodel. Deelrapport4: Extra aanpassingen Zeeschelde. WL Rapporten, 753_09. Flanders Hydraulics Research, Antwerp, Belgium. Retrieved from https://www.vliz.be/imisdocs/publications/237561.pdf.

Maximova, T., Ides, S., Vanlede, J., De Mulder, T., & Mostaert, F. (2009). LTV O&M thema Veiligheid Deelproject 1: Verbetering 2D randvoorwaardenmodel. Deelrapport 3: Kalibratie bovenlopen. WL Rapporten, 753_09. Flanders Hydraulics Research, Antwerp, Belgium. Available at https://www.vliz.be/imisdocs/publications/36/155036.pdf.

Meadows, D. H., & Wright, D. (2009). *Thinking in systems: A primer*: London: Earthscan.

Passeri, D. L., Hagen, S. C., Medeiros, S. C., Bilskie, M. V., Alizad, K., & Wang, D. (2015). Earth's future special section: The dynamic effects of sea level rise on low-gradient coastal landscapes: A review. *Earth's Future*, *3*, 159–181. https://doi.org/10.1002/2015EF000298

Pethick, J. S. (1981). Long-term accretion rates on tidal salt marshes. *Journal of Sedimentary Petrology*, *51*, 571–577. https://doi.org/10.1306/212F7CDE-2B24-11D7-8648000102C1865D

Pritchard, D., Hogg, A. J., & Roberts, W. (2002). Morphological modelling of intertidal mudflats: The role of cross-shore tidal currents. *Continental Shelf Research*, *22*, 1887–1895. https://doi.org/10.1016/S0278-4343(02)00044-4

Ris, R. C., Holthuijsen, L. H., & Booij, N. (1999). A third-generation wave model for coastal regions: 2. Verification. *Journal of Geophysical Research*, *104*, 7667–7681.

Roberts, W., Le, Hir, & Whitehouse, R. J. S. (2000). Investigation using simple mathematical models of the effect of tidal currents and waves on the profile shape of intertidal mudflats. *Continental Shelf Research*, *20*, 1079–1097. https://doi.org/10.1016/S0278-4343(00)00013-3

Roelvink, J. A. (2006). Coastal morphodynamic evolution. *Coastal Engineering*, *53*(2-3), 277–287. https://doi.org/10.1016/j.coastaleng.2005.10.015

Sampath, D. M. R., Boski, T., Silva, P. L., & Martins, F. A. (2011). Morphological evolution of the Guadiana estuary and intertidal zone in response to projected sea-level rise and sediment supply scenarios. *Journal of Quaternary Science*, *26*(2), 156–170. https://doi.org/10.1002/jqs.1434

Syvitski, J. P., Vrsmarty, C. J., Kettner, A. J., & Green, P. (2005). Impact of humans on the flux of terrestrial sediment to the global coastal ocean. *Science*, *308*(5720), 376–380. https://doi.org/10.1126/science.1109454

Tambroni, N., & Seminara, G. (2012). A one-dimensional eco-geomorphic model of marsh response to sea level rise: Wind effects, dynamics of the marsh border and equilibrium. *Journal of Geophysical Research*, *117*, F03026. https://doi.org/10.1029/2012JF002363

van Goor, M. A., Zitman, T. J., Wang, Z. B., & Stive, M. J. F (2003). Impact of sea-level rise on the morphological equilibrium state of tidal inlets. *Marine Geology*, *202*(3-4), 211–227. https://doi.org/10.1016/S0025-3227(03)00262-7

van Maanen, B., Coco, G., & Bryan, K. R. (2015). On the ecogeomorphological feedbacks that control tidal channel network evolution in a sandy mangrove setting. *Proceedings of the Royal Society A*, *471*(2180). https://doi.org/10.1098/rspa.2015.0115

van Maanen, B., Coco, G., Bryan, K. R., & Friedrichs, C. T. (2013). Modeling the morphodynamic response of tidal embayments to sea-level rise. *Ocean Dynamics*, *63*, 1249–1262. https://doi.org/10.1007/s10236-013-0649-6

van de Kam, J., Battley, P. F., McCaffery, B. J., Rogers, D. I., Hong, J. S., Moores, N., et al. (2010). Invisible connections: Why migrating shorebirds need the Yellow Sea. *South Australian Ornithologist*, *37*(1).

van der Wal, D., van Kessel, T., Eleveld, M. A., & Vanlede, J. (2010). Spatial heterogeneity in estuarine mud dynamics. *Ocean Dynamics*, *60*, 519–533. https://doi.org/10.1007/s10236-010-0271-9

van der Wegen, M., Jaffe, B., Foxgrover, A., & Roelvink, D. (2017). Mudflat morphodynamics and the impact of sea level rise in South San Francisco Bay. *Estuaries and Coasts*, *40*(1), 37–49. https://doi.org/10.1007/s12237-016-0129-6

Waeles, B., Le Hir, P., & Jacinto, R. S. (2004). Modelisation morphodynamique cross-shore d'un estran vaseux. *Comptes Rendus Geoscience*, *336*, 1025–1033. https://doi.org/10.1016/j.crte.2004.03.011

Wang, Z. B., Van Maren, D. S., Ding, P. X., Yang, S. L., van Prooijen, B. C., De Vet, P. L. M., et al. (2015). Human impacts on morphodynamic thresholds in estuarine systems. *Continental Shelf Research*, *111*, 174–183. https://doi.org/10.1016/j.csr.2015.08.009

Wiegmann, N., Perluka, R., Oude Elberink, S., & Vogelzang, J. (2005). Vaklodingen: de inwintechnieken en hun combinaties: Vergelijking tussen verschillende inwintechnieken en de combinaties ervan Technical Report Adviesdienst Geo-Informatica en ICT (AGI) Delft (in Dutch).

Winterwerp, J. C., & Van Kesteren, W. G. (2004). Introduction to the physics of cohesive sediment dynamics in the marine environment, *Developments in Sedimentology* (56 pp.). Amsterdam: Elsevier.

Zhou, Z., Coco, G., Townend, I., Olabarrieta, M., van der Wegen, M., Gong, Z., et al. (2017). Is "morphodynamic equilibrium" an oxymoron? *Earth-Science Reviews*, *165*, 257–267. https://doi.org/10.1016/j.earscirev.2016.12.002

Zhu, Q. (2017). Sediment dynamics on intertidal mudflats: A study based on in situ measurements and numerical modelling. https://doi.org/10.4233/uuid:5f094e4b-fef9-4216-abbe-3277adc90b28